


Article

An Improved Droop Control Strategy for Low-Voltage Microgrids Based on Distributed Secondary Power Optimization Control

Demin Li ¹ , Bo Zhao ², Zaijun Wu ^{1,*}, Xuesong Zhang ² and Leiqi Zhang ²¹ School of Electrical Engineering, Southeast University, Nanjing 210096, China; llied_min@163.com² State Grid Zhejiang Electric Power Research Institute, Hangzhou 310014, China; zhaobozju@163.com (B.Z.); ee_zxs@163.com (X.Z.); zhangleiqi@zju.edu.cn (L.Z.)

* Correspondence: zjwu@seu.edu.cn; Tel.: +86-25-8379-4163 (ext. 602)

Received: 1 August 2017; Accepted: 1 September 2017; Published: 7 September 2017

Abstract: To achieve accurate reactive power sharing and voltage frequency and amplitude restoration in low-voltage microgrids, a control strategy combining an improved droop control with distributed secondary power optimization control is proposed. The active and reactive power that each distributed generator (DG) shares is calculated by extracting load information and utilizing a power sharing ratio, and is reset to be the nominal power to recalculate droop gains. The droop control curves are reconstructed according to the nominal active and reactive power and the recalculated droop gains. The reconstructed active power-frequency droop control can regulate active power adaptively and keep frequency at a nominal value. Meanwhile, the reconstructed reactive power voltage droop control can reduce voltage amplitude deviation to a certain extent. A distributed secondary power optimization control is added to the reconstructed reactive power voltage droop control by using average system voltage. The average system voltage is obtained by using a consensus algorithm in a distributed, sparse communication network which is constituted by all controllers of DGs. As a result, accurate reactive power sharing is realized, average system voltage is kept at a nominal value, and all voltage amplitude deviations are further reduced. Due to the absence of a microgrid central controller, the reliability of the strategy is enhanced. Finally, the simulation results validate the proposed method.

Keywords: low-voltage microgrids; improved droop control; distributed secondary power optimization control; consensus algorithm; accurate reactive power sharing

1. Introduction

In a microgrid, the distributed generator (DG) units are interfaced with the alternating current (AC) network via power converters. The operation features of converter-based DGs are different with the conventional synchronous generators, such as fast response and low inertia [1–4].

A microgrid can work in both grid-connected and islanded modes [5]. Hierarchical control is generally implemented for microgrids to standardize their operation and functionalities [6–9]. Three control levels are defined in the hierarchical control frame. Primary control is the first level, and droop control is generally used to achieve the target of plug-and-play operation for microgrids [10–12]. The conventional droop control cannot keep voltage amplitude and frequency at nominal values. In addition, the accuracy of reactive power sharing is poor due to line impedance [13–15]. To improve the reactive power sharing accuracy, a method based on small harmonic signal injection has been proposed in [16]. However, this method may decrease system stability and bring about line current distortions [17]. In [18–20], a virtual impedance loop is designed to improve the reactive power sharing accuracy.

Adding secondary control to the primary control is an effective strategy to ensure accurate power sharing. The centralized secondary control approach is based on communication network relays using a microgrid central controller (MGCC). An MGCC acts as a secondary loop in islanding mode and improves power sharing accuracy by measuring parameters at certain points of the microgrid [21–24]. Although accurate power sharing is achieved, each DG has a strong dependency upon MGCC. With the feature of good expansibility and reliability, distributed control can relieve communication burden and act as an important mean to reduce dependence on central node [25–31]. In [29], a distributed control based on consensus algorithm is referenced to study the coordination control among DGs under different starting time.

In this paper, a control strategy combining an improved droop control with distributed secondary power optimization control is proposed. Each DG is assigned with a distributed controller (DCr) and each load is assigned with a load controller (LCr). LCr collects load information and transfers them to the neighboring DCrs. All DCrs constitute a distributed sparse communication network. The global load information is obtained by exchanging load information in the network. The active and reactive power that each DG shares is calculated by using the global load information and power sharing ratio, and is reset to be the nominal power to recalculate droop gains. The improved droop control curves are reconstructed according to the nominal power and the recalculated droop gains. Each DG outputs active and reactive power and regulates voltage amplitude and frequency according to the improved droop control curves. Accurate active power sharing is realized and frequency is always kept at nominal value. Compared with [26,32], secondary frequency control is omitted.

Although the improved Q - E droop control is implemented, the output reactive power among DGs is disproportional to the power sharing ratio due to the effect of line impedance, and therefore voltage drop is inevitable. To further reduce voltage amplitude deviation and realize accurate reactive power sharing, a distributed secondary power optimization control based on a consensus algorithm is added to the improved Q - E droop control. Each DCr can exchange voltage information with neighboring controllers, and the average system voltage for secondary optimization control is obtained with a consensus algorithm. With the combination of the improved Q - E droop control and distributed secondary power optimization control, accurate reactive power sharing is realized; meanwhile, all output voltage amplitude deviations are further reduced, and average system voltage is kept at the nominal value. Due to the absence of MGCC, reliability is enhanced.

This paper is organized as follows. In Section 2, the conventional droop control is briefly introduced and reactive power sharing among inverters is analyzed under the effect of line impedance. The improved droop control curves utilizing load information and power sharing ratio are constructed in Section 3. In Section 4, average system voltage is obtained with a consensus algorithm. Accurate reactive power sharing is realized by adding distributed secondary control to the improved Q - E droop control, and average system voltage is kept at a nominal value. The simulation results are presented in Section 5. Finally, Section 6 concludes the paper.

2. Conventional Droop Control and Reactive Power Sharing Analysis

A typical AC microgrid is illustrated in Figure 1. The output voltage of the i th DG (DG_i) is $E_i \angle \varphi_i$ ($i = 1, 2, \dots, N$), where E_i and φ_i are the voltage amplitude and voltage phase, respectively. The voltage of point of common coupling (PCC) is $E_{com} \angle \varphi_{com}$. $Z_i \angle \varphi_{Zi} = R_i + jX_i$ represents the line impedance between DG_i and PCC, where R_i , X_i are line resistance, inductance, respectively. $P_i + jQ_i$ represents output power of DG_i , where P_i , Q_i are active and reactive power, respectively. I_{oi} is the output current of DG_i . P_i and Q_i can be expressed in Equation (1):

$$\begin{cases} P_i = \frac{E_i^2 \cos \varphi_{Zi} - E_i E_{com} \cos(\varphi_i - \varphi_{com} + \varphi_{Zi})}{Z_i} \\ Q_i = \frac{E_i^2 \sin \varphi_{Zi} - E_i E_{com} \sin(\varphi_i - \varphi_{com} + \varphi_{Zi})}{Z_i} \end{cases} \quad (1)$$

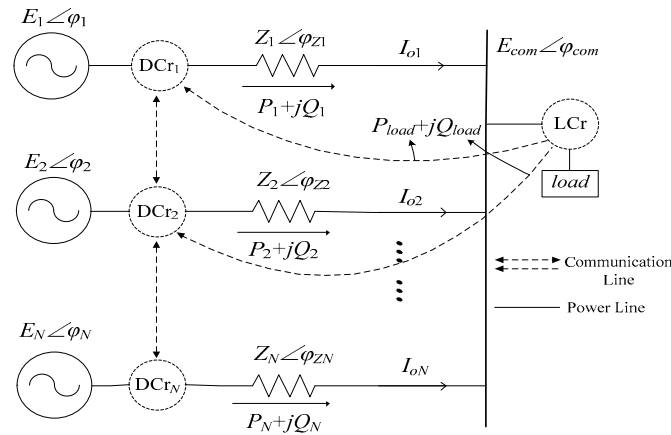


Figure 1. Equivalent model of many sets of distributed generators connected in parallel.

The line impedance is predominantly resistive ($R \gg X$) in a low-voltage microgrid. Without loss of generality, the minor line reactance is neglected in the study [33], so that $Z_i \approx R_i$, $\varphi_{zi} \approx 0^\circ$, $\cos \varphi_{zi} \approx 1$, and $\sin \varphi_{zi} \approx \varphi_{zi}$. Thus, Equation (1) can be simplified as (2)

$$\begin{cases} P_i \approx \frac{E_i^2 - E_i E_{com} \cos \theta_i}{R_i} \\ Q_i \approx \frac{-E_i E_{com} \sin \theta_i}{R_i} \end{cases} \quad (2)$$

where θ_i is the power angle between the output voltage of DG_i and the voltage of PCC, $\theta_i = \varphi_i - \varphi_{com} = 2\pi \int (f_i - f_{com}) dt$, f_i is the frequency of output voltage of DG_i , and f_{com} is the voltage frequency of PCC.

The effectiveness of conventional P - f and Q - E droop control applied in a low-voltage microgrid is verified in [32] and the control equations for DG_i are described in Equation (3):

$$\begin{cases} f_i^* = f_n + m_i (P_{ni} - P_i) \\ E_i^* = E_n + n_i (Q_{ni} - Q_i) \end{cases} \quad (3)$$

where E_i^* and f_i^* are referenced voltage amplitude and frequency of DG_i . E_n and f_n are normal voltage amplitude and frequency. P_{ni} and Q_{ni} are the set-points for the active and reactive power of DG_i , and m_i , n_i are droop gains in active and reactive power droop control, respectively.

The conventional P - f and Q - E droop characteristics are drawn by the solid lines in Figures 2 and 3, respectively. The output active power is P_{ni} when frequency is f_n as shown by point A in Figure 2. The output reactive power is Q_{ni} when voltage amplitude is E_n as shown by point A' in Figure 3. The operating point moves to point B or point B' when load varies, and frequency or voltage amplitude deviates from a nominal value. The frequencies of all DGs operated in parallel are equal at steady state ($f_i = f_j = f$, $i \neq j$). Hence, $m_i (P_{ni} - P_i) = m_j (P_{nj} - P_j)$ is obtained in Equation (3) with the P - f droop. m_i and m_j are chosen to satisfy $m_i P_{ni} = m_j P_{nj}$, then $P_i : P_j = (1/m_i) : (1/m_j)$, so that each DG shares the active power in proportional to power sharing ratio. The power angle θ_i is generally small, thus, the active power in Equation (2) is approximated as [33]

$$P_i \approx \frac{E_{com} (E_i - E_{com})}{R_i} \quad (4)$$

where P_i is approximated as the delivered active power of DG_i into the common bus.

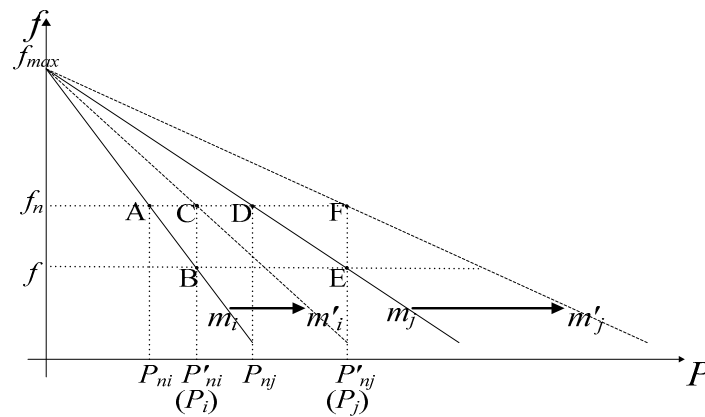


Figure 2. Conventional and improved P - f droop control characteristics.

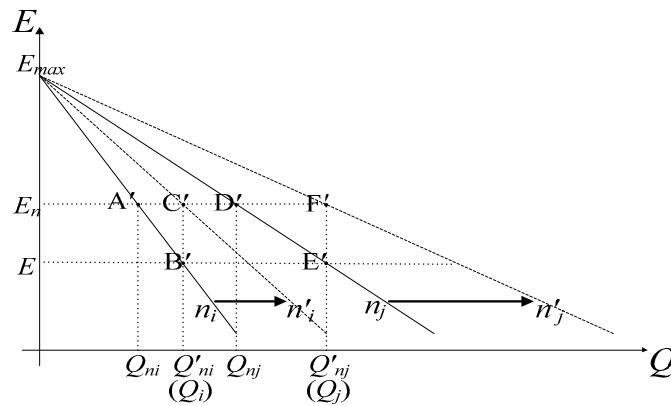


Figure 3. Conventional and improved Q - E droop control characteristics.

From Equation (4), the voltage magnitude difference ($E_i - E_{com}$) can be expressed as

$$E_i - E_{com} \approx \frac{P_i R_i}{E_{com}} \quad (5)$$

Assuming that $E_i^* \approx E_i$ and substituting E_i^* in Equation (3) into Equation (5) yields

$$Q_i \approx \frac{E_n - E_{com}}{n_i} - \frac{P_i R_i}{n_i E_{com}} + Q_{ni} \quad (6)$$

The reactive power sharing error of any two DGs within a microgrid is defined as

$$\Delta Q = \frac{Q_i}{Q_{ni}} - \frac{Q_j}{Q_{nj}} \approx \underbrace{\left(\frac{E_n - E_{com}}{n_i Q_{ni}} - \frac{E_n - E_{com}}{n_j Q_{nj}} \right)}_{\text{First error term}} + \underbrace{\left(\frac{P_j R_j}{n_j E_{com} Q_{nj}} - \frac{P_i R_i}{n_i E_{com} Q_{ni}} \right)}_{\text{Second error term}} \quad (7)$$

From Equation (7), the reactive power sharing error of two DGs includes two terms. The first error term predominantly depends on the voltage magnitude difference ($E_n - E_{com}$). When $n_i Q_{ni} = n_j Q_{nj}$ is satisfied, the first term is zero. The second error term is mainly determined by line resistances and active powers. However, allocating a certain ratio is difficult among actual line impedances, so that $P_i R_i = P_j R_j$ is difficult to be realized and the second error term is not identically zero. Thus, the output reactive power among two DGs has a sharing error and accurate reactive power sharing is not accomplished.

3. Improved Droop Control Strategy

In Figure 2, when DG_i operating at point B, the output frequency is f , and frequency deviation is Δf ($\Delta f = |f_n - f|$). This section reconstructs droop control curves to reduce frequency and voltage amplitude deviations. Ignoring the effect of line impedance, DG_i operates from point A to B as shown in Figure 2 or point A' to B' as shown in Figure 3 when load varies. The output active and reactive power is P_i and Q_i , respectively. Let $P'_{ni} = P_i$ and $Q'_{ni} = Q_i$. If (P'_{ni}, f_n) be defined as a new nominal operating point, as shown by point C in Figure 2, and an improved P - f droop control curve is reconstructed by connecting the no-load operating point and point C, as the dotted line shown in Figure 2, the droop gain of which is m'_i . Similarly, (Q'_{ni}, E_n) is defined as a new nominal operating point, and an improved Q - E droop control curve is reconstructed as the dotted line containing point C' shown in Figure 3, the droop gain of which is n'_i . The improved droop control formulas are illustrated in Equation (8):

$$\begin{cases} f_i^* = f_n + m'_i(P'_{ni} - P_i) \\ E_i^* = E_n + n'_i(Q'_{ni} - Q_i) \end{cases} \quad (8)$$

If $m'_i P'_{ni} = m_i P_{ni}$ and $n'_i Q'_{ni} = n_i Q_{ni}$, then $f_n + m'_i P'_{ni} = f_n + m_i P_{ni} = f_{max}$ and $E_n + n'_i Q'_{ni} = E_n + n_i Q_{ni} = E_{max}$. The improved droop control gains m'_i, n'_i are illustrated in Equation (9):

$$\begin{cases} m'_i = \frac{m_i P_{ni}}{P'_{ni}} \\ n'_i = \frac{n_i Q_{ni}}{Q'_{ni}} \end{cases} \quad (9)$$

At first, we assume that the system operating in point B corresponds to point B' in Figure 3. Starting the improved droop strategy, DG_i moves to point C, corresponding to point C'. The output active power of DG_i is $P_i, P_i = P'_{ni}$. The output reactive power is $Q_i, Q_i = Q'_{ni}$. Meanwhile, the frequency and voltage amplitude are restored at nominal values.

Ignoring the effect of line impedance, we assume that two arbitrary DGs operate in parallel, i.e., DG_i and DG_j , run at nominal points as shown by points A and D in Figure 2, corresponding to points A' and D' in Figure 3. When load varies, the two DGs operate at point B (B') and E (E') respectively. Let $P'_{ni} = P_i, Q'_{ni} = Q_i, P'_{nj} = P_j$ and $Q'_{nj} = Q_j$. If (P'_{ni}, f_n) and (Q'_{ni}, E_n) are defined as new nominal operating points as shown by points C and C'; similarly, (P'_{nj}, f_n) and (Q'_{nj}, E_n) as the new nominal operating points as shown by points F and F', then the improved droop gains m'_i, n'_i, m'_j and n'_j are chosen to satisfy Equation (10):

$$\begin{cases} m_i P_{ni} = m'_i P'_{ni} = m'_j P'_{nj} = m_j P_{nj} \\ n_i Q_{ni} = n'_i Q'_{ni} = n'_j Q'_{nj} = n_j Q_{nj} \end{cases} \quad (10)$$

where m'_i, n'_i, m'_j and n'_j are obtained according to Equation (9), such as $m'_j = (m_j P_{nj})/P'_{nj}$ and $n'_j = (n_j Q_{nj})/Q'_{nj}$. The improved P - f droop control curves are reconstructed as dotted lines containing C and F, respectively, shown in Figure 2. Similarly, the improved Q - E droop control curves are reconstructed as dotted lines containing C' and F', respectively, shown in Figure 3.

Starting the improved droop strategy, DG_i operates from point B (B') to C (C'), DG_j operates from point E (E') to F (F'). The proportional equation $P_i:P_j = P'_{ni}:P'_{nj} = (1/m'_i):(1/m'_j) = (1/m_i):(1/m_j)$ is satisfied, and $Q'_{ni}:Q'_{nj} = Q_i:Q_j = (1/n'_i):(1/n'_j) = (1/n_i):(1/n_j)$. The frequencies and voltage amplitudes are restored at nominal values.

N DG units operated in parallel are extended to analyze the improved droop control strategy when ignoring the effect of line impedance. Let $P'_{ni} = P_i$ and $Q'_{ni} = Q_i, i = 1, 2, \dots, N$. m'_i and $n'_i, i = 1, 2, \dots, N$, are chosen to satisfy Equation (11):

$$\begin{cases} m'_1 P'_{n1} = m'_2 P'_{n2} = \dots = m'_N P'_{nN} = m_1 P_{n1} = m_2 P_{n2} = \dots = m_N P_{nN} \\ n'_1 Q'_{n1} = n'_2 Q'_{n2} = \dots = n'_N Q'_{nN} = n_1 Q_{n1} = n_2 Q_{n2} = \dots = n_N Q_{nN} \end{cases} \quad (11)$$

where m'_i, n'_i are obtained according to Equation (9). The power sharing ratio satisfies Equation (12):

$$\begin{cases} P'_{n1} : P'_{n2} : \dots : P'_{nN} = P_1 : P_2 : \dots : P_N = \frac{1}{m'_1} : \frac{1}{m'_2} : \dots : \frac{1}{m'_N} = \frac{1}{m_1} : \frac{1}{m_2} : \dots : \frac{1}{m_N} \\ Q'_{n1} : Q'_{n2} : \dots : Q'_{nN} = Q_1 : Q_2 : \dots : Q_N = \frac{1}{n'_1} : \frac{1}{n'_2} : \dots : \frac{1}{n'_N} = \frac{1}{n_1} : \frac{1}{n_2} : \dots : \frac{1}{n_N} \end{cases} \quad (12)$$

The power sharing ratio among DGs is generally given by the tertiary control level; i.e., $(1/m_1):(1/m_2): \dots :(1/m_N)$ and $(1/n_1):(1/n_2): \dots :(1/n_N)$ are given in advance. The initial values of m_i, n_i , are also given. To calculate m'_i and n'_i , P'_{ni} and Q'_{ni} should be obtained. The process of obtaining global load information by all DCrS is elaborated in Section 4. If the global load is expressed as $P_{load} + jQ_{load}$, then it is shared by all DGs, i.e., $P_{load} = P'_{n1} + P'_{n2} + \dots + P'_{nN}$, $Q_{load} = Q'_{n1} + Q'_{n2} + \dots + Q'_{nN}$. The i th DCr (DCr _{i}) calculates the active and reactive power that DG _{i} shares as follows:

$$\begin{cases} P'_{ni} = \frac{1/m_i}{\sum_{i=1}^N (1/m_i)} P_{load} = G_{Pi} P_{load} \\ Q'_{ni} = \frac{1/n_i}{\sum_{i=1}^N (1/n_i)} Q_{load} = G_{Qi} Q_{load} \end{cases} \quad i = 1, 2, \dots, N \quad (13)$$

where G_{Pi} and G_{Qi} are power sharing coefficients of DG _{i} , $0 < G_{Pi} < 1$, and $0 < G_{Qi} < 1$. DCr _{i} calculates P'_{ni} and Q'_{ni} according to Equation (13), then substituting them into Equation (9) to obtain m'_i and n'_i . Finally, Equation (8) is constructed. The active power sharing ratio is $(1/m_1):(1/m_2): \dots :(1/m_N)$. Similarly, $Q_1:Q_2: \dots :Q_N = (1/n_1):(1/n_2): \dots :(1/n_N)$. Meanwhile, $f_1^* = f_2^* = \dots = f_N^* = f_n$, and $E_1^* = E_2^* = \dots = E_N^* = E_n$. When load varies, DCr obtains new P_{load} and Q_{load} . Then, P'_{ni} and Q'_{ni} are recalculated. m'_i and n'_i are obtained and droop control curves are reconstructed. The methods for calculating the variation of droop gains have been given in [34] and the relevant conclusions of eigenvalue analysis have existed, so it is not covered here. Thus, accurate power sharing is always realized, and voltage amplitude and frequency are always kept at nominal values.

The above analysis results are obtained without considering the effect of line impedance. When considering line impedance, the voltage drops across different line impedances are not equal, resulting in the output voltages also not being equal. Thus, the target of reactive power sharing in Equation (12) is difficult to realize.

4. Distributed Secondary Power Optimization Control Based on a Consensus Algorithm

To eliminate the effect of line impedance, a distributed secondary power optimization control is added to the improved Q-E droop control in this section. The average system voltage is obtained by using a discrete consensus algorithm via a distributed sparse communication network which is composed of all DCrS. The simplified distributed sparse communication network is shown in Figure 4. Each DCr is regarded as a node and each node can exchange voltage or load information with neighboring nodes (referring to other nodes that exchange with the node as the neighboring nodes). Two arbitrary nodes exchange information in a bidirectional way. Since an LCr merely transfers load information to the neighboring DCrS in a unidirectional way, as shown in Figure 5 or Figure 6, and do not participate in exchanging voltage information, the distributed sparse communication network does not include LCrS. In Figure 4, DCr₂ obtains status information from DCr₁ and DCr_N by exchanging information with them. Meanwhile, DCr₂ can also transfer the status information of DCr_N to DCr₁; thus, DCr₁ obtains the status information of DCr_N indirectly. Finally, any status information is obtained by all nodes, e.g., LCr₁ transfers the local load information ($load_1: P_{load1} + jQ_{load1}$) to DCr₁ in Figure 6. DCr₁ transfers the information of $load_1$ to DCr₂, and DCr₂ transfers them to DCr₃, then all DCrS obtain the information of $load_1$. Similarly, all DCrS can obtain the information of $load_2$ and $load_3$. Then, each DCr obtains the global load information by adding all local load information.

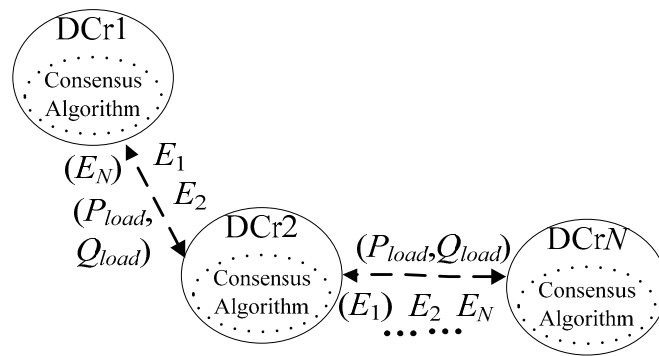


Figure 4. Distributed sparse communication network.

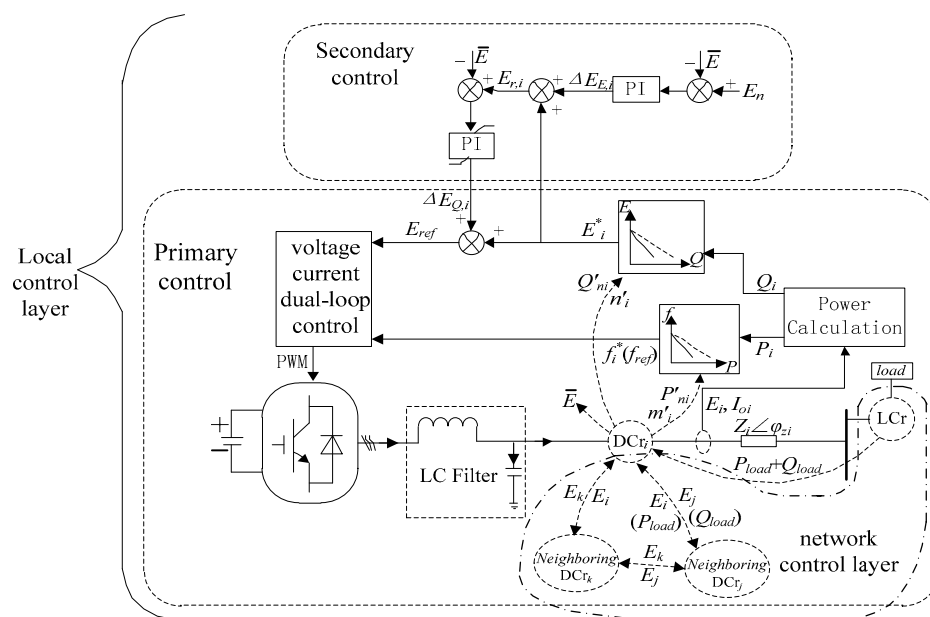


Figure 5. Structure of distributed secondary power optimization control based on the improved droop control strategy.

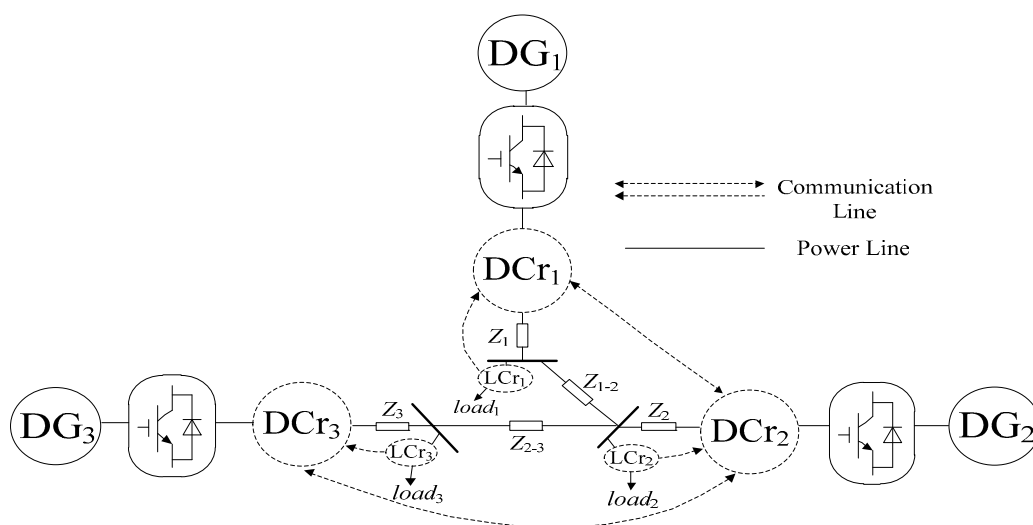


Figure 6. Structure of the AC microgrid.

4.1. Discrete Consensus Algorithm

With the feature of simple convergence conditions and fast convergence rate [35–38], the first order discrete consensus algorithm is used to obtain average system voltage. In Figure 4, the state variables of DCR_{*i*} (*i* = 1, 2, . . . , *N*) is expressed as *x_i*. When the state variables of all nodes are equal or the state variable error is less than the given accuracy, the system reaches consensus convergence by using consensus algorithm. The first-order continuous consensus algorithm is expressed as:

$$\dot{x}_i(t) = u_i(t), \quad i = 1, 2, \dots, N \quad (14)$$

where *u_i(t)* is the input variable of node *i* and expressed as follows:

$$u_i(t) = - \sum_{j \in N_i} a_{ij}(x_i(t) - x_j(t)), \quad i = 1, 2, \dots, N \quad (15)$$

where *a_{ij}* is the coefficient for information exchanged between nodes *i* and *j*. If nodes *i* and *j* are connected through a distribution line, $0 < a_{ij} < 1$; otherwise, *a_{ij}* = 0. *N_i* is the indexes of nodes that are connected to node *i* [36]. This system can concisely be expressed as follows:

$$\dot{X} = -L_N X \quad (16)$$

where *X* is the system state variable vector composed of *x_i*. *L_N* is *N* × *N* order Laplacian matrix and determined by network topology. The actual system is usually a discrete control system; hence, the first-order discrete consensus algorithm is introduced to analyze system dynamic characteristics.

$$x_i[k+1] = \sum_{j=1}^N d_{ij}x_j[k], \quad i = 1, 2, \dots, N \quad (17)$$

Equation (17) is expressed in matrix form:

$$X^{k+1} = DX^k \quad (18)$$

where *d_{ij}* is the element of matrix *D*. If all elements of matrix *D* are nonnegative and the sums of each row and column are all ones i.e., $D^*e = e$ and $D^T e = e$, with $e = [1, 1, \dots, 1]^T$, then *D* is called the doubly stochastic matrix [37], and the system would reach consensus convergence at the average value of state variables, i.e.,

$$\lim_{k \rightarrow \infty} X^k = \lim_{k \rightarrow \infty} D^k X^0 = \frac{ee^T}{N} X^0 \quad (19)$$

where *X⁰* is the system initial state variable vector.

An improved *Metropolis* method was proposed in [38] to construct *D*, which is expressed in Equation (20), where $\max(n_i, n_j)$ is the maximum number of neighbors among node *i* and its neighboring nodes. If convergence accuracy ε is given, then Equation (21) expresses iterations.

$$d_{ij} = \begin{cases} \frac{1}{[\max(n_i, n_j)+1]} & j \in N_i \\ 1 - \sum_{j \in N_i} \frac{1}{[\max(n_i, n_j)+1]} & i = j \\ 0 & \text{otherwise} \end{cases} \quad (20)$$

$$K = \frac{-1}{\log_{\varepsilon} \left(\frac{1}{|\lambda_2|} \right)} \quad (21)$$

where λ_2 is the second largest eigenvalue of *D*. However, λ_2 may vary with the change of network structure. The accurate value of *K* is hard to be obtained by applying Equation (21). If the state error

of the k th iteration is less than ε , i.e., Equation (22) is satisfied, it can be concluded that a consensus convergence has been reached.

$$\sum_{i=1}^N |x_i[k] - x_i[k-1]| < \varepsilon \quad (22)$$

4.2. Distributed Secondary Power Optimization Control Based on a Discrete Consensus Algorithm

The structure of distributed secondary power optimization control based on improved droop control strategy is illustrated in Figure 5, which contains a local control layer and network control layer. The local control layer consists of primary control and secondary control. Primary control contains an inverter, output filter, power calculation block, the improved droop control block, voltage and current dual-loop control block, and a DC microsource. Secondary control is added to the improved Q-E droop control to optimize reactive power. The network control layer contains DCr and LCr, and is used for transferring load information and exchanging voltage information, meanwhile, using a consensus algorithm to calculate average system voltage, as shown in the dotted line area. Since the frequency is restored at f_n and not affected by line impedance, the proposed control strategy in Figure 5 merely needs the reactive power secondary control to optimize reactive power sharing, and the secondary frequency control is no longer needed compared to [26,32]. Meanwhile, output voltage amplitude deviations are further reduced via secondary control, which is illustrated in this section and the simulation results of Section 5.1.

The flow chart of first order discrete consensus algorithm is illustrated in Figure 7. Setting a synchronous sampling clock and its sampling period is T_s . Let $t = kT_s$; each LCr extracts local load information and transfers them to the neighboring DCr when $k = 0$. Each DCr extracts voltage information driven by the clock signal and puts them in the local state variable ($x_i[0]$), then exchanges voltage information with neighboring DCrs. Meanwhile, each DCr exchanges local load information with neighboring DCrs and calculates the global load information, then puts them in $P_{load}[0]$ and $Q_{load}[0]$. m'_i , n'_i , P'_{ni} and Q'_{ni} are calculated, respectively. At the next clock signal, $x_i[k+1]$ is calculated by using Equation (16), and the state error of the k th iteration is obtained according to Equation (21). If the state error is greater than or equal to ε , then the iteration repeats. Otherwise, the outputting consensus convergence results are taken to be the average system voltage, i.e., \bar{E} and resetting $k = 0$. When the next clock signal arrives, each DCr obtains load information and judges $P_{load}[k]$ with $P_{load}[k-1]$. If $P_{load}[k] = P_{load}[k-1]$, each DCr keeps the m'_i and P'_{ni} of the last clock signal; otherwise, they recalculate m'_i and P'_{ni} . Similarly, they judge $Q_{load}[k]$ with $Q_{load}[k-1]$ and recalculate n'_i and Q'_{ni} when $Q_{load}[k]$ is not equal to $Q_{load}[k-1]$.

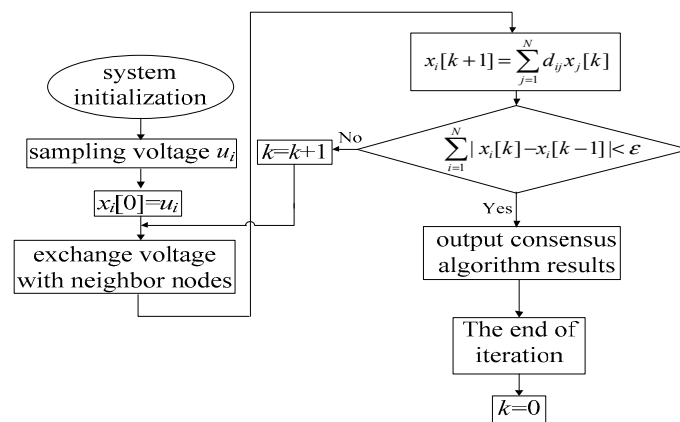


Figure 7. Flow chart of the discrete consensus algorithm.

We assume that the output voltage amplitudes of all DGs are equal at steady state, i.e., $E_1 = E_2 = \dots = E_N = \bar{E}$. According to Equation (8),

$$n'_i Q_i = E_n + n'_i Q'_{ni} - \bar{E}, \quad i = 1, 2, \dots, N \quad (23)$$

$E_i[k]$ is the output voltage of DCr_i at k th iteration, $x_i[0] = E_{i,0}$. If Equation (22) is satisfied, $E_i[k]$ is set to be \bar{E} applied in DG_i, i.e., $\bar{E} = E_i[k]$. The values of $(n'_i Q'_{ni} + E_n - \bar{E})$ are equal for all DGs, then $n'_i Q_i$ are also equal. Hence, the output reactive power is not affected by line impedance, and the relationships of reactive power sharing in Equations (11) and (12) are satisfied. To satisfy the prerequisites of $E_i = \bar{E}$, $i = 1, 2, \dots, N$, $(E_n + n'_i Q'_{ni} - n'_i Q_i)$ is regulated via a Proportional and Integral (PI) controller:

$$\Delta E_{Q,i} = (k_{PQ} + \frac{k_{IQ}}{s})[(E_n + n'_i Q'_{ni} - n'_i Q_i) - \bar{E}] = (k_{PQ} + \frac{k_{IQ}}{s})[(E_n + n'_i Q'_{ni} - \bar{E}) - n'_i Q_i] \quad (24)$$

where $\Delta E_{Q,i}$ is the regulating variable of reactive power control, k_{PQ} and k_{IQ} are proportional and integral gains of the reactive power PI controller. Substituting Q-E droop control formula in Equation (8) into Equation (24) yields

$$\Delta E_{Q,i} = (k_{PQ} + \frac{k_{IQ}}{s})(E_i - \bar{E}) \quad (25)$$

To make E_i equals to \bar{E} , the reference voltage of DG_i is regulated by adding $\Delta E_{Q,i}$ to E_i^* . Due to the effect of line impedance, the average system voltage has a voltage drop even if the improved Q-E droop control is adopted. To keep \bar{E} at E_n , regulating \bar{E} via a voltage PI controller:

$$\Delta E_{E,i} = (k_{PE} + \frac{k_{IE}}{s})(E_n - \bar{E}), \quad i = 1, 2, \dots, N \quad (26)$$

where k_{PE} and k_{IE} are proportional and integral gains of the voltage PI controller. Both the reactive power PI controller and voltage PI controller regulate the reference voltage of Q-E droop control to realize the control target. Merging Equations (25) and (26) yields

$$E_{ref} = E_i^* + \Delta E_{Q,i} = E_i^* + (k_{PQ} + \frac{k_{IQ}}{s})(E_{r,i} - \bar{E}), \quad i = 1, 2, \dots, N \quad (27)$$

where $E_{r,i} = E_i^* + \Delta E_{E,i}$.

5. Simulation Results

A low-voltage microgrid with three DGs is built based on Matlab R2014a/Simulink, which is shown in Figure 6. $Z_i (i = 1, 2, 3)$ represents the line impedance between DG_i and PCC. $Z_{i-j} (i, j = 1, 2, 3, i \neq j)$ represents the line impedance among different common buses. The initial parameters are shown in Table 1. r_f , L_f , and C_f of LC filter are 0.1 Ω , 1.35 mH and 50 μ F, respectively. Both the active and reactive power sharing ratio are 3:2:2, i.e., $P_{n1}:P_{n2}:P_{n3} = Q_{n1}:Q_{n2}:Q_{n3} = 3:2:2$. The matrix D is constructed according to Equation (20) and is expressed in Equation (28). $f_n = 50$ Hz and $E_n = 311$ V. The system stability is affected by the sampling period [38]. To improve system stability, the sampling period is set to be 0.5 ms in this paper, i.e., $T_s = 0.5$ ms.

$$D = \begin{bmatrix} 1/3 & 1/3 & 1/3 \\ 1/3 & 2/3 & 0 \\ 1/3 & 0 & 2/3 \end{bmatrix} \quad (28)$$

Table 1. Parameters of the model.

DG	P-f Droop Gain $m_{i,0}$ (Hz/kW)	Q-E Droop Gain $n_{i,0}$ (V/kVar)	Rated Active Power $P_{ni,0}$ (kW)	Rated Reactive Power $Q_{ni,0}$ (kVar)	Load	Values	Line Impedance	Values
DG ₁	0.0556	1.4286	9	10.5	Load ₁ /KVA	$9 + j10$	Z_1/Ω	$0.2 + j0.031$
DG ₂	0.0833	2.1429	6	7	Load ₂ /KVA	$8.5 + j11$	Z_2/Ω Z_3/Ω	$0.3 + j0.063$ $0.2 + j0.031$
DG ₃	0.0833	2.1429	6	7	Load ₃ /KVA	$7 + j7$	Z_{1-2}/Ω Z_{2-3}/Ω	$0.4 + j0.063$ $0.5 + j0.094$

5.1. Case A: Disturbance Analysis

This simulation can be divided into four stages:

Stage 1 (0–1 s): The conventional droop control shown in Equation (3) is used to control the 3 DGs in Figure 6. Load 1 and Load 2 are connected to the system at $t = 0$ s.

Stage 2 (1–2 s): The improved droop control shown in Equation (8) is used to control the 3 DGs at $t = 1$ s.

Stage 3 (2–3 s): The secondary power optimization control is added to the improved Q-E droop control to optimize reactive power and regulate voltage amplitude at $t = 2$ s.

Stage 4 (3–4 s): Load 3 is connected to the system at $t = 3$ s.

The state error accuracy ε is set to be 0.01. The simulation results are shown in Figure 8. The active and reactive power are illustrated in Figure 8a,b, respectively. The output frequency and voltage amplitude are illustrated in Figure 8c,d, respectively. Figure 8e shows the k th iterative voltage of DCr _{i} in the process of discrete consensus algorithm, i.e., $E_i[k]$. During stage 1, the frequencies of all DGs are equal and deviating from 50 Hz as seen from Figure 8c. The active powers are 7.49 kW, 5.01 kW, 5 kW, respectively, i.e., $P_1:P_2:P_3 = 3:2:2$, as seen from Figure 8a. The reactive power cannot be shared in proportional to 3:2:2 and $Q_2 \neq Q_3$ as seen from Figure 8b. Figure 8d illustrates the output voltages of DG₁, DG₂ and DG₃ are 313.6 V, 313.7 V and 312.4 V, respectively, and the average system voltage is 313.23 V. Both output voltages and average system voltage deviate from 311 V.

Starting the improved droop control at $t = 1$ s. During stage 2, the voltage frequencies of all DGs are restored to be 50 Hz, shown in Figure 8c. The active powers are 7.5 kW, 5 kW, 5 kW, respectively. The output voltages are 311.3 V, 311.3 V and 310.6 V, respectively, and $\bar{E} = 311.07$ V. Thus, output voltage amplitude deviations are reduced, but accurate reactive power sharing is still not realized. Figure 8b shows the reactive power sharing ratio is not 3:2:2 and $Q_2 \neq Q_3$.

The secondary control is added to the improved Q-E droop control at $t = 2$ s. During stage 3, the reactive powers are 8.97 kVar, 5.97 kVar, 5.98 kVar shown in Figure 8b, and the sharing ratio is 3:2:2. Figure 8d shows the voltages are 311.12 V, 311.1 V and 310.78 V, respectively, and $\bar{E} = 311$ V. It reveals that accurate reactive power sharing is achieved, and voltage amplitude deviations are further reduced compared with Stage 2. Figure 8e shows that the three output voltages of DCr _{s} are equal to 311 V after several iterative calculations. Load 3 is connected to the system at $t = 3$ s. At first, the active and reactive power sharing accuracies are decreased. The system reaches a steady state after a short time adjustment. During Stage 4, the frequencies of all DGs are 50 Hz. Figure 8d shows the voltages are 310.7 V, 311.15 V and 311.15 V, respectively, and $\bar{E} = 311$ V. Figure 8a shows P_1 , P_2 , P_3 are 10.49 kW, 6.99 kW, 6.99 kW, and the sharing ratio is 3:2:2. Figure 8b shows Q_1 , Q_2 , Q_3 are 11.96 kVar, 7.97 kVar, 7.98 kVar, and the sharing ratio is also 3:2:2.

Figure 8 shows that the proposed control strategy, combining the improved droop control with distributed secondary power optimization control, can share active and reactive power in proportion to the power sharing ratio. Meanwhile, the frequencies of all DGs and average system voltage are kept at nominal values, and the output voltage amplitude deviations are all reduced.

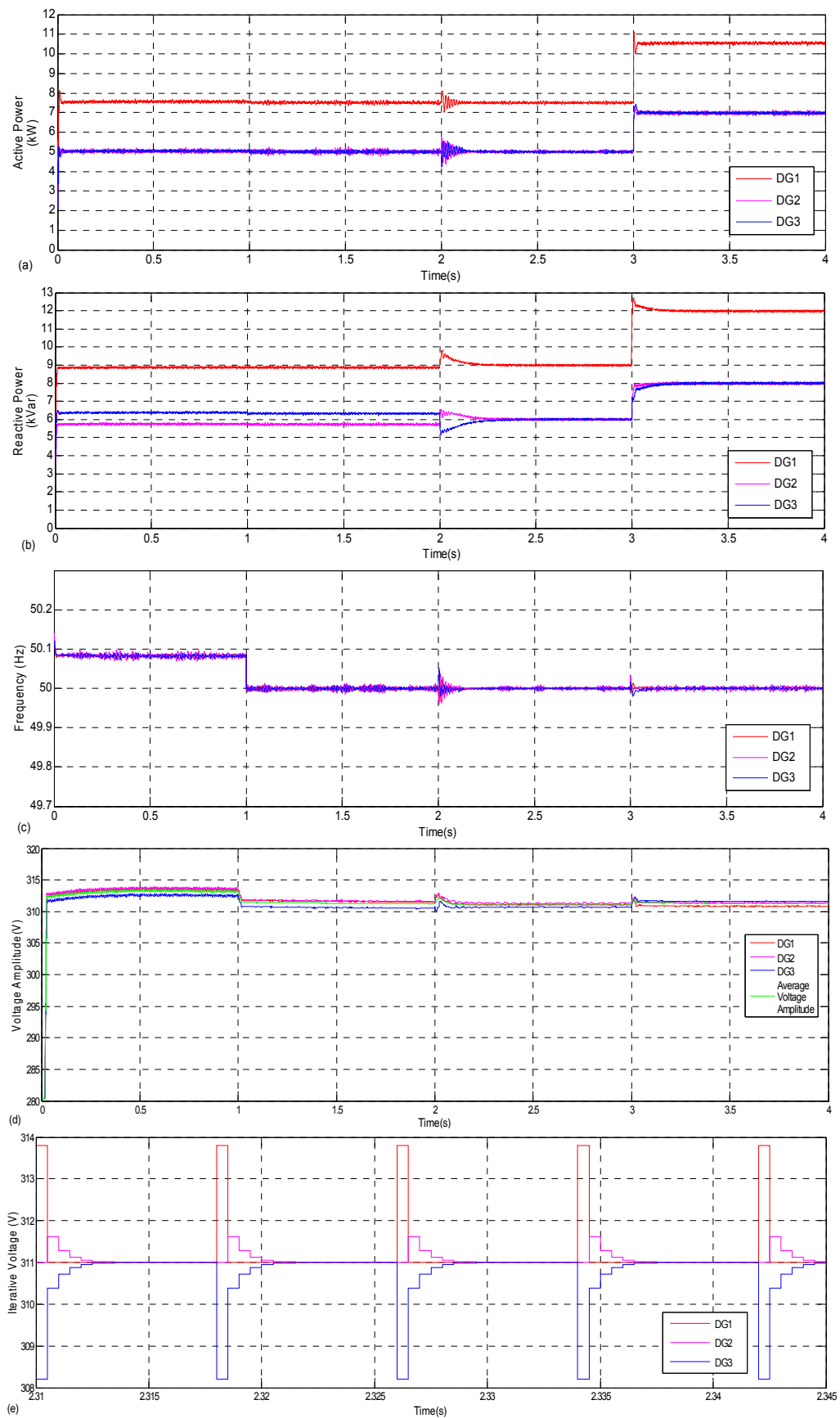


Figure 8. Simulation results in Case A: (a) active power; (b) reactive power; (c) frequency; (d) output voltage amplitude and average voltage amplitude; and (e) iterative voltage amplitude.

5.2. Case B: Variations of Line Impedance

Four sets of scenario simulations with different line impedances are designed according to the microgrid model shown in Figure 6. Loads 1 and 2 are connected to the system and the reactive power sharing ratio is 3:2:2. The line impedances of all groups are shown in Table 2. Group 1 uses the conventional droop control shown in Equation (3) to regulate all DGs. Groups 2, 3 and 4 use the improved droop control combined with secondary control to regulate all DGs. The reactive powers, output voltages and the corresponding deviations are shown in Table 3. The average voltage deviation is the deviation between average system voltage and 311 V. The average reactive power deviation is designed as

$$e_Q = \left(\frac{1}{3} \sum_{i=1}^3 \left| \frac{Q'_i}{Q'_{ni}} - 1 \right| \right) \times 100\% \quad (29)$$

Table 2. Parameters of line impedance in different groups.

Groups	Z_1/Ω	Z_2/Ω	Z_3/Ω	Z_{1-2}/Ω	Z_{2-3}/Ω
Group 1	$0.2 + j0.031$	$0.4 + j0.063$	$0.3 + j0.063$	$0.5 + j0.063$	$0.4 + j0.063$
Group 2	$0.2 + j0.031$	$0.4 + j0.063$	$0.3 + j0.031$	$0.5 + j0.063$	$0.4 + j0.063$
Group 3	$0.3 + j0.063$	$0.3 + j0.063$	$0.2 + j0.031$	$0.6 + j0.094$	$0.5 + j0.063$
Group 4	$0.2 + j0.031$	$0.3 + j0.063$	$0.2 + j0.031$	$0.4 + j0.063$	$0.5 + j0.094$

Table 3. System steady-state operation results in different groups.

Groups	Parameters	DG ₁	DG ₂	DG ₃
Group 1	Reactive Power/kVar	8.86	5.61	6.37
	Voltage/V	313.1	314	313.2
	$e_Q/\%$		4.741	
	Average Voltage Deviation/V		2.433	
Group 2	Reactive Power/kVar	8.99	5.98	5.99
	Voltage/V	310.5	311.2	311.3
	$e_Q/\%$		0.204	
	Average Voltage Deviation/V		0	
Group 3	Reactive Power/kVar	8.98	5.99	5.99
	Voltage/V	311.7	311.1	310.3
	$e_Q/\%$		0.185	
	Average Voltage Deviation/V		0.033	
Group 4	Reactive Power/kVar	8.99	5.98	6.00
	Voltage/V	310.7	311.4	310.9
	$e_Q/\%$		0.148	
	Average Voltage Deviation/V		0	

Table 3 reveals that the reactive power sharing ratio is not 3:2:2 in Group 1; meanwhile, both average voltage deviation and average reactive power deviation are larger than the simulation results in Groups 2, 3 and 4. The e_Q of Groups 2, 3 and 4 are 0.204%, 0.185% and 0.148%, respectively. The average voltage deviations of Groups of 2, 3 and 4 are 0 V, 0.033 V and 0 V, respectively. The line impedances in Group 1 and Group 2 are equal, and the two groups' simulation results reveal that the control strategy proposed in this paper can share reactive power accurately in proportional to the sharing ratio; meanwhile, the average system voltage is kept at nominal value and all output voltage deviations are reduced. Groups 2, 3 and 4 reveal that the accurate reactive power sharing is

not affected by line impedance variations and the average system voltage can be kept at nominal value under different line impedances.

5.3. Case C: Influence of Different Convergence Accuracies

Equation (21) shows that the iterations vary when convergence accuracies (ε) change. The higher the accuracy or the smaller the ε , the more iterations. Thus, it takes a long time to calculate average value. On the contrary, the lower the accuracy, the fewer iterations. Three sets of scenario simulations with the effect of different ε are designed. The ε are 0.1, 0.01 and 0.001, respectively. The reactive power sharing ratio is 3:2:2. Load 1 and Load 2 are connected to the system at $t = 0$ s. Load 3 is connected to the system at $t = 0.5$ s. The different output voltages of DCr_{*i*} via consensus algorithm and the corresponding voltage convergence deviations are shown in Table 4. The voltage convergence deviation is designed as:

$$e_E = \frac{1}{3} \sum_{i=1}^3 \left| \frac{E_i}{E_{ave}} - 1 \right| \quad (30)$$

where E_i is the output voltage of DCr_{*i*} via consensus algorithm, E_{ave} is the average output iterative voltage.

Table 4. Convergence results and deviations under different convergence accuracies.

ε	E_i/V			$e_E/\times 10^{-3}$
	DCr1	DCr2	DCr3	
0.1	311.0752	311.1621	311.1132	0.0970
0.01	310.9923	311.0126	310.9857	0.0337
0.001	310.9931	310.9951	310.9937	0.0024

From Table 4, the e_E with ε is 0.1 is larger than the values of e_E with ε are 0.01 and 0.001. The e_E is 0.0337×10^{-3} when ε is 0.01, which is larger than the e_E with ε is 0.001. Table 4 reveals that the smaller the ε , the smaller the voltage convergence deviation. From Figure 9a, Q_2 is not equal to Q_3 when ε is 0.1. This reveals that accurate reactive power sharing is not realized when the convergence accuracy is low. From Figure 9b,c, the target of accurate reactive power sharing in proportional to 3:2:2 is realized when ε is 0.01 or 0.001. Comparing Figure 9b,c the adjustment process with ε is 0.01 is more smooth when the process with ε is 0.001 at $t = 0.5$ s. The adjustment process appears to overshoot at $t = 0.5$ s when ε is 0.001. This is due to a high convergence accuracy requiring more iterations, thus prolonging iteration time. It takes a long time to update the output iterative voltage, resulting in the output iterative voltage cannot be timely used by secondary Q-E droop control, thus the transient performance is reduced.

From the above analysis, the smaller the ε is given, the more iterations and the longer iteration time are needed. Although the convergence accuracy is improved, the transient performance is reduced. On the contrary, the target of accurate reactive power sharing cannot be realized when the convergence accuracy is too low. Therefore, both the accurate reactive power sharing ratio and transient performance are considered to set the ε reasonably. The ε is set to be 0.01 in Sections 5.1 and 5.2 to guarantee accurate reactive power sharing and smooth transient performance.

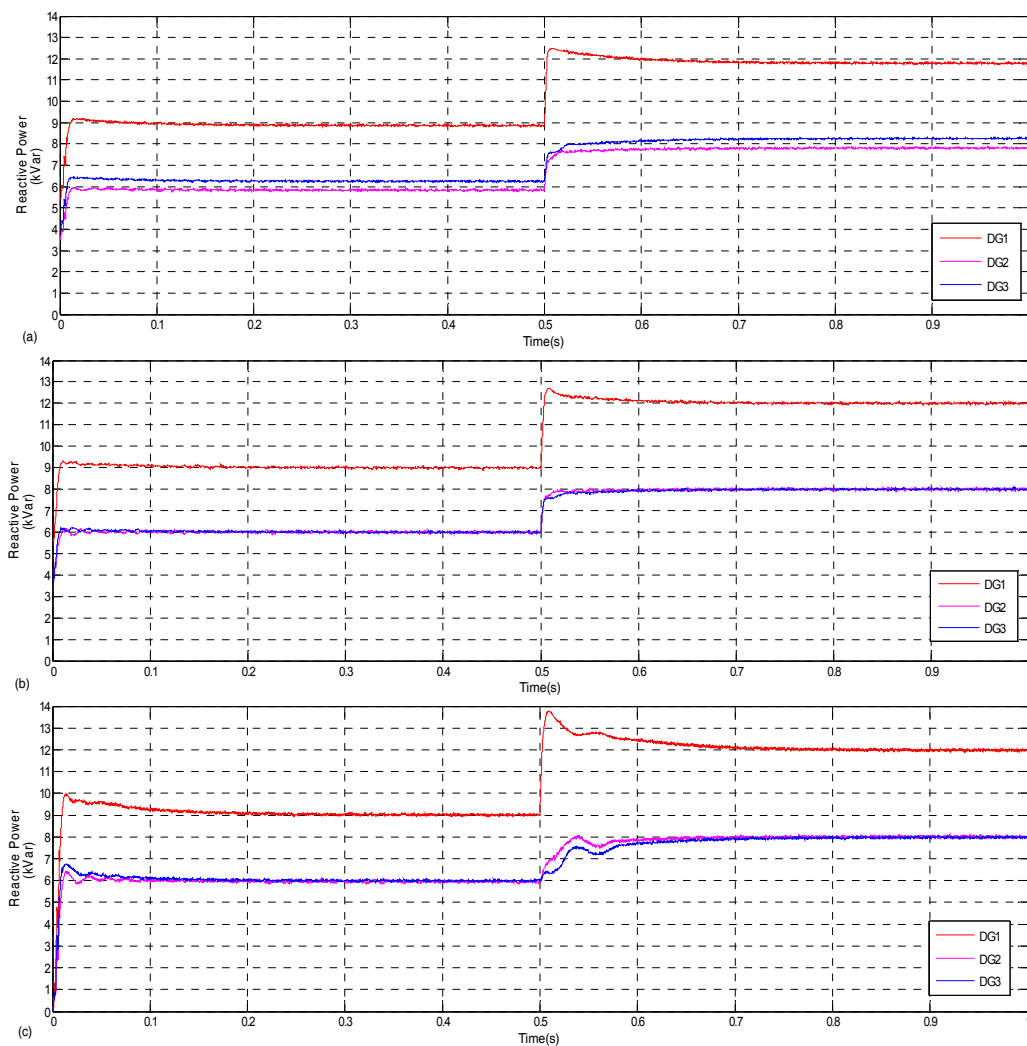


Figure 9. Simulation results in Case C: (a) reactive power with ε is 0.1; (b) reactive power with ε is 0.01; and (c) reactive power with ε is 0.001.

5.4. Case D: Influence of Communication Delay

Section 4 shows that each DCr updates voltage or load information every other sampling period (T_s). If a DCr obtains load information exceeding the time of a sampling period, then the load information cannot be timely used by a DCr. This section discusses the influence of different time delays in communication system. If the communication delay is τ , i.e., a DCr or LCr sends information after τ milliseconds of the arrival of the clock signal, then the interval time that a DCr updates information or a LCr transfers load information to the neighboring DCrs is Δt ($\Delta t = T_s + \tau$). The τ are 0.05 ms, 0.25 ms and 0.5 ms, respectively. The reactive power sharing ratio is 3:2:2. ε is 0.01. Load 1 and Load 2 are connected to the system at $t = 0$ s. Different simulation results are shown in Figure 10.

Figure 10a shows that the starting process appears to overshoot when τ is 0.05 ms, which is similar to Figure 9c. This is due to the fact that relevant information, such as average system voltage, cannot be utilized in a timely fashion as a result of communication delay. Figure 10b shows that the output reactive powers appear largely fluctuations when τ is 0.25 ms. Figure 10c shows that the simulation results are oscillatory and the system is unstable when τ is 0.5 ms. The simulation results reveal that the dynamic output performance of the microgrid would be deteriorated when a delay exists in the communication system, and that the excessive communication delay would result in system instability.

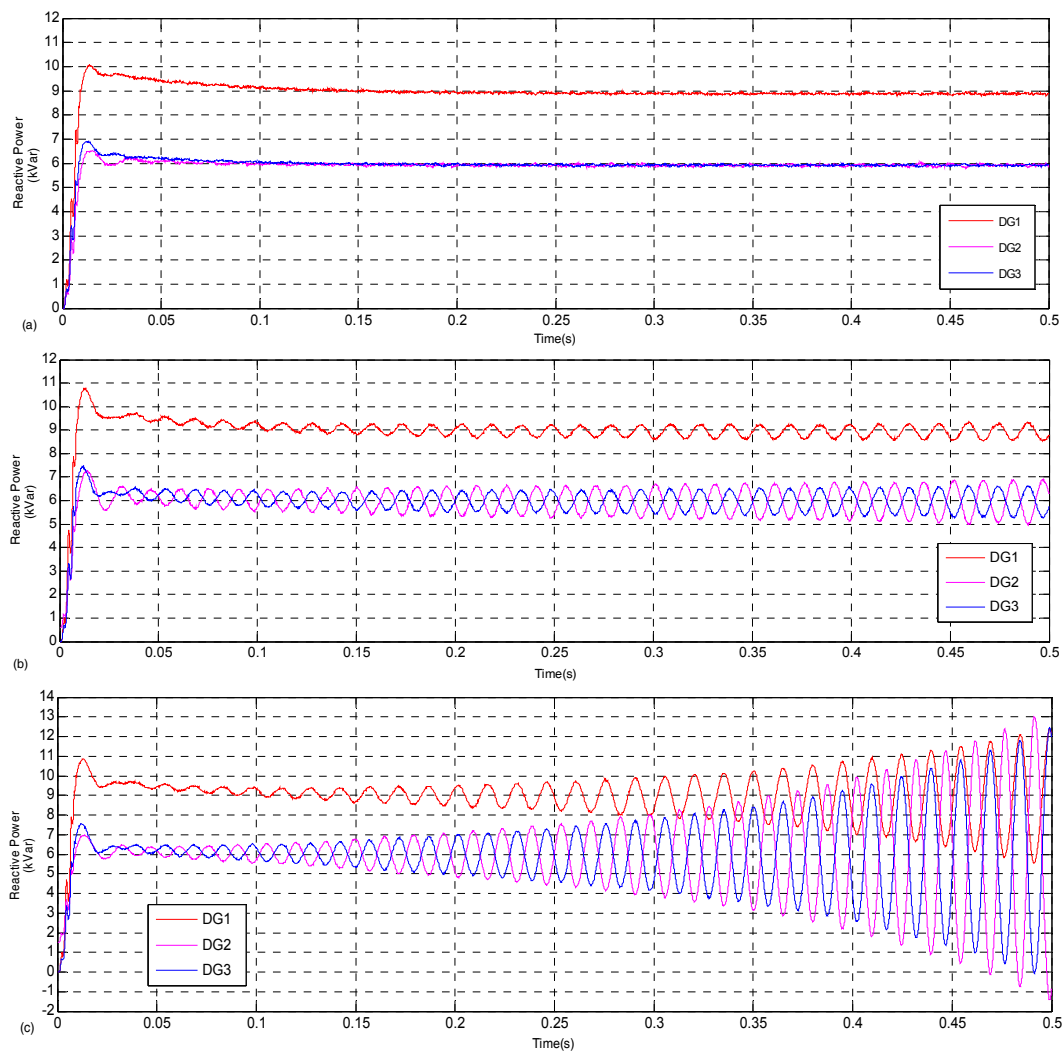


Figure 10. Simulation results in Case D: (a) reactive power with τ is 0.05ms; (b) reactive power with τ is 0.25ms; and (c) reactive power with τ is 0.5ms.

6. Conclusions

A control strategy combining an improved droop control which can regulate droop gains with distributed secondary power optimization control is proposed. The improved P - f droop control can always keep frequency at a nominal value when load varies without secondary frequency control; meanwhile, sharing the active power in proportion to the power sharing ratio. The distributed secondary reactive power optimization control based on a consensus algorithm is added to the improved Q - E droop control. With the control strategy, average system voltage is kept at a nominal value and the output voltage amplitude deviations of all DGs are reduced to a large extent. Meanwhile, the target of accurate reactive power sharing in proportion to the power sharing ratio is realized. The reasonable value of the convergence accuracy (ϵ) used in the consensus algorithm is determined by simulation to satisfy both accurate reactive power sharing and transient performance. The simulation results also reveal that accurate reactive power sharing is not affected by line impedance variations and that excessive communication delay would result in system instability. The control strategy based on a distributed sparse communication network does not need MGCC, which gives the strategy a good reliability. The simulation results have also verified its effectiveness.

Acknowledgments: This work was supported by National High Technology Research and Development Program of China (No. 2015AA050104) and supported by the Key R&R Program of Jiangsu province (BE2015012-1).

Author Contributions: Demin Li conceived the main idea, performed simulations, and wrote the manuscript. Zaijun Wu and Bo Zhao contributed to developing the ideas in this research. Xuesong Zhang and Leiqi Zhang thoroughly revised the paper.

Conflicts of Interest: The authors declare no conflict of interest.

References

1. Wang, H.; Huang, J. Joint Investment and Operation of Microgrid. *IEEE Trans. Smart Grid* **2017**, *8*, 833–845. [[CrossRef](#)]
2. Golsorkhi, M.S.; Lu, D.D.C. A control method for inverter-based islanded microgrids based on V-I droop characteristics. *IEEE Trans. Power Deliv.* **2015**, *30*, 1196–1204. [[CrossRef](#)]
3. Ahn, C.; Peng, H. Decentralized and real-time power dispatch control for an islanded microgrid supported by distributed power sources. *Energies* **2013**, *6*, 6439–6454. [[CrossRef](#)]
4. Katiraei, F.; Iravani, M.R.; Lehn, P.W. Microgrid autonomous operation during and subsequent to islanding process. *IEEE Trans. Power Deliv.* **2005**, *20*, 248–257. [[CrossRef](#)]
5. Yu, Z.; Ai, Q.; He, X.; Piao, L. Adaptive droop control for microgrids based on the synergetic control of multi-agent systems. *Energies* **2016**, *9*, 1057. [[CrossRef](#)]
6. Guerrero, J.M.; Vasquez, J.C.; Matas, J.; Vicuna, L.G.D.; Castilla, M. Hierarchical control of droop-controlled AC and DC microgrids—A General Approach Toward Standardization. *IEEE Trans. Ind. Electron.* **2011**, *58*, 158–172. [[CrossRef](#)]
7. Bidram, A.; Davoudi, A. Hierarchical structure of microgrids control system. *IEEE Trans. Smart Grid* **2012**, *3*, 1963–1976. [[CrossRef](#)]
8. Parhizi, S.; Lotfi, H.; Khodaei, A.; Bahramirad, S. State of the art in research on microgrids: A review. *IEEE Access* **2015**, *3*, 890–925. [[CrossRef](#)]
9. Lu, X.; Guerrero, J.M.; Sun, K.; Vasquez, J.C.; Teodorescu, R.; Huang, L. Hierarchical control of parallel AC-DC converter interfaces for hybrid microgrids. *IEEE Trans. Smart Grid* **2014**, *5*, 683–692. [[CrossRef](#)]
10. Patterson, M.; Macia, N.F.; Kannan, A.M. Hybrid microgrid model based on solar photovoltaic battery fuel cell system for intermittent load applications. *IEEE Trans. Energy Convers.* **2015**, *30*, 359–366. [[CrossRef](#)]
11. Dragicevic, T.; Guerrero, J.M.; Vasquez, J.C.; Škrlec, D. Supervisory control of an adaptive-droop regulated dc Microgrid with battery management capability. *IEEE Trans. Ind. Electron.* **2014**, *29*, 695–706. [[CrossRef](#)]
12. Egwebe, A.M.; Fazeli, M.; Igic, P.; Holland, P.M. Implementation and stability study of dynamic droop in islanded microgrids. *IEEE Trans. Energy Convers.* **2016**, *31*, 821–832. [[CrossRef](#)]
13. Guo, F.; Wen, C.; Mao, J.; Song, Y. Distributed secondary voltage and frequency restoration control of droop-controlled inverter-based microgrids. *IEEE Trans. Ind. Electron.* **2015**, *62*, 4355–4364. [[CrossRef](#)]
14. Guerrero, J.M.; Matas, J.; de Vicuña, L.G. Decentralized control for parallel operation of distributed generation inverters using resistive output impedance. *IEEE Trans. Ind. Electron.* **2007**, *54*, 994–1004. [[CrossRef](#)]
15. Gu, W.; Liu, W.; Wu, Z.; Zhao, B.; Chen, W. Cooperative control to enhance the frequency stability of islanded microgrids with DFIG-SMES. *Energies* **2013**, *6*, 3951–3971. [[CrossRef](#)]
16. Tuladhar, A.; Jin, H.; Unger, T.; Mauch, K. Control of parallel inverters in distributed AC power systems with consideration of line impedance effect. *IEEE Trans. Ind. Appl.* **2000**, *36*, 131–138. [[CrossRef](#)]
17. Li, Y.; Kao, C.-N. An accurate power control strategy for power-electronics-interfaced distributed generation units operating in a low-voltage multibus microgrid. *IEEE Trans. Power Electron.* **2009**, *24*, 2977–2988.
18. Guerrero, J.M.; Vicuna, L.G.D.; Matas, J.; Castilla, M.; Miret, J. Out impedance design of parallel-connected UPS inverters with wireless load-sharing control. *IEEE Trans. Ind. Electron.* **2005**, *52*, 1126–1135. [[CrossRef](#)]
19. He, J.; Li, Y. Analysis, design, and implementation of virtual impedance for power electronics interfaced distributed generation. *IEEE Trans. Ind. Appl.* **2011**, *47*, 2525–2538. [[CrossRef](#)]
20. Zhu, Y.; Zhuo, F.; Wang, F.; Liu, B.; Gou, R.; Zhao, Y. A virtual impedance optimization method for reactive power sharing in networked microgrid. *IEEE Trans. Power Electron.* **2016**, *31*, 2890–2904. [[CrossRef](#)]
21. Majumder, R.; Ledwich, G.; Ghosh, A. Droop control of converter-interfaced microsources in rural distributed generation. *IEEE Trans. Power Deliv.* **2010**, *25*, 2768–2778. [[CrossRef](#)]

22. Hajizadeh, A.; Golkar, M.A. Intelligent power management strategy of hybrid distributed generation system. *Int. J. Electr. Power Energy Syst.* **2007**, *29*, 783–795. [[CrossRef](#)]
23. Wang, C.; Yang, X.; Wu, Z.; Che, Y.; Guo, L.; Zhang, S.; Liu, Y. A Highly integrated and reconfigurable microgrid testbed with hybrid distributed energy sources. *IEEE Trans. Smart Grid* **2016**, *7*, 451–459. [[CrossRef](#)]
24. Yao, W.; Chen, M.; Matas, J.; Guerrero, J.M.; Qian, Z. Design and analysis of the droop control method for parallel inverters considering the impact of the complex impedance on the power sharing. *IEEE Trans. Ind. Electron.* **2011**, *58*, 576–588. [[CrossRef](#)]
25. Ahn, S.J.; Nam, S.R.; Choi, J.H.; Moon, S.I. Power scheduling of distributed generators for economic and stable operation of a microgrid. *IEEE Trans. Smart Grid* **2013**, *4*, 398–405. [[CrossRef](#)]
26. Shafiee, Q.; Guerrero, J.M.; Vasquez, J.C. Distributed secondary control for islanded microgrids—A novel approach. *IEEE Trans. Power Electron.* **2014**, *29*, 1018–1030. [[CrossRef](#)]
27. Nasirian, V.; Davoudi, A.; Lewis, F.L.; Guerrero, J.M. Distributed adaptive droop control for DC distribution systems. *IEEE Trans. Energy Convers.* **2014**, *29*, 944–956. [[CrossRef](#)]
28. Zhong, Q. Robust droop controller for accurate proportional load sharing among inverters operated in parallel. *IEEE Trans. Ind. Electron.* **2013**, *60*, 1281–1290. [[CrossRef](#)]
29. Wu, D.; Dragicevic, T.; Vasquez, J.C.; Guerrero, J.M. Secondary coordinated control of islanded microgrids based on consensus algorithms. In Proceedings of the Energy Conversion Congress and Exposition (ECCE), Pittsburgh, PA, USA, 14–18 September 2014; pp. 4290–4297.
30. Vandoorn, T.L.; Kooning, J.D.M.D.; Vyver, J.V.D.; Vandevelde, L. Three-Phase Primary Control for Unbalance Sharing between Distributed Generation Units in a Microgrid. *Energies* **2013**, *6*, 6586–6607. [[CrossRef](#)]
31. Mohamed, Y.; El-Saadany, E.F. Adaptive decentralized droop controller to preserve power sharing stability of paralleled inverters in distributed generation microgrids. *IEEE Trans. Power Electron.* **2008**, *23*, 2806–2816. [[CrossRef](#)]
32. Savaghebi, M.; Jalilian, A.; Vasquez, J.C.; Guerrero, J.M. Secondary Control Scheme for Voltage Unbalance Compensation in an Islanded Droop-Controlled Microgrid. *IEEE Trans. Smart Grid* **2012**, *3*, 797–807. [[CrossRef](#)]
33. Hou, X.; Sun, Y.; Yuan, W.; Zhong, C. Conventional $P-\omega/Q-V$ droop control in highly resistive line of low-voltage converter-based AC microgrid. *Energies* **2016**, *9*, 943. [[CrossRef](#)]
34. Hatano, Y.; Mesbahi, M. Agreement over random networks. *IEEE Trans. Autom. Control* **2005**, *50*, 1867–1872. [[CrossRef](#)]
35. Pogaku, N.; Prodanovic, M.; Green, T.C. Modeling, Analysis and Testing of Autonomous Operation of an Inverter-Based Microgrid. *IEEE Trans. Power Electron.* **2007**, *22*, 613–625. [[CrossRef](#)]
36. Khoo, S.; Xie, L.; Man, Z. Robust Finite-Time Consensus Tracking Algorithm for Multirobot Systems. *IEEE/ASME Trans. Mechatron.* **2009**, *14*, 219–228. [[CrossRef](#)]
37. Xu, Y.; Liu, W. Novel multiagent based load restoration algorithm for microgrids. *IEEE Trans. Smart Grid* **2011**, *2*, 152–161. [[CrossRef](#)]
38. Zhang, Z.; Chow, M.Y. Convergence analysis of the incremental cost consensus algorithm under different communication network topologies in a smart grid. *IEEE Trans. Power Syst.* **2012**, *27*, 1761–1768. [[CrossRef](#)]

